Sensors and Actuators A 315 (2020) 112356

Contents lists available at ScienceDirect

Sensors and Actuators A: Physical

journal homepage: www.elsevier.com/locate/sna

Scalable pendulum energy harvester for unmanned surface vehicles

James Graves, Yang Kuang*, Meiling Zhu*

College of Engineering, Mathematics and Physical Sciences, University of Exeter, Exeter, EX4 4QF, UK

ARTICLE INFO

Article history:
Received 14 April 2020
Received in revised form 4 August 2020
Accepted 11 September 2020
Available online 29 September 2020

Keywords:
Energy harvesting
Vibration
Electromagnetic
Pendulum
Mechanical rotation
Rectifier
Wave energy

ABSTRACT

This paper proposes a novel pendulum energy harvester design for converting energy of low frequency ambient vibration, such as that found in unmanned surface vehicles (USVs) due to ocean waves, into usable electrical energy. The primary novelty of this design is the mechanical rotation rectifier (MRR) system, which is able to improve on existing designs through the use of spur gears and sprag clutches capable of handling significant torque, in an arrangement which is easily scalable to larger devices. Using a minimal number of offset gears, this system is designed to maintain high efficiency and minimal backlash. The energy harvester was proven to produce a maximum normalised average power output of 20.62 W/g^2, corresponding to an average power of 0.72 W and a power density of 0.43 W/kg, at 0.186 g rms acceleration. The resonant frequency of the system is designed at 1 Hz, within the range of the expected natural frequencies of USV motion. The energy conversion efficiency at resonance was 43.5 %. Furthermore, a mathematical model was developed and verified through experimental testing, and was used to simulate the effects of various pendulum lengths, masses and flywheels on the system. This demonstrates the specific negative relationship between pendulum arm length and natural frequency of the system, as well as the positive correlation between pendulum mass and maximum power. Furthermore, higher inertia flywheels are shown to produce significantly smoothed voltages and increased output power, while extending the time it takes for the harvester to reach steady state. It is concluded that this device would be viable for assisting in powering USV communications and extending the exploration life of these vessels.

1. Introduction

With an ever increasing concern for the future state of the planet, there is significant demand for the ability to monitor wildlife and climate across the globe. There are, however, parts of the sea where exploration and recording of data are difficult, leading to the heightened prevalence of unmanned surface vehicles (USVs). While such vessels can operate for days or weeks with batteries or fuel cells, these have finite capacity, and solar can be useful but long-term operation in the often dark Arctic and Antarctic oceans is yet out of reach. Energy harvesting from the vibration of these vessels, generated by ocean waves, could provide an alternative source of power to greatly extend their period of operation.

The electric power source of this type of vessel is used for sensors and navigation. The requirement can vary depending on the size and function of the vessels. Existing research has shown the demands for similar vessels to be in the range of multiple watts [1]. A study by Yin et al. [2] assesses the natural frequencies of various sized ships, and shows that these lies in the range of approximately 0.5–3.5 Hz in the vertical direction. While there has been significant research into the use of piezoelectric [3–6], triboelectric [7,8] and small electromagnetic [9–13] transducers for harvesting ambient vibration, electromagnetic energy harvesters utilising electric motors as generators are most likely to be capable of producing this high power demand [14–16]. A large proportion of existing small-scale electromagnetic designs for surface wave energy harvesters involve one part of the system being submerged, with another section floating on the surface, and energy extracted from the varying displacement with time between the two [17,18]. While this can be very effective for buoys and other fixed-position structures, having such a device submerged in the water would create substantial drag on a moving vessel, and hence is not practical for USV use. Therefore, there is a need to study inertial vibration energy harvesters for converting wave energy, such that a device can be developed to fit within the hull of a USV.

Small-scale inertial wave vibration energy harvesting frequently comes in the form of floating buoys [18]. These buoys often rely upon vertical single-axis vibration perpendicular to the wave fronts, and there are many electromagnetic energy harvesters

* Corresponding authors.
E-mail addresses: y.kuang@exeter.ac.uk (Y. Kuang), m.zhu@exeter.ac.uk (M. Zhu).

https://doi.org/10.1016/j.sna.2020.112356

which have been designed for harvesting this type of excitation [19–21], including the use of dual mass systems [22]. One such mechanism was designed by Rome et al. [23], using the vertical motion of a 38 kg backpack during walking to produce 7.4 W of power. As well as those designed for vertical motion, a number of devices harvest the pitch and roll of vessels. Townsend [1] designed a gyroscopic energy harvester for use in autonomous underwater vehicles, using a motor driven flywheel to amplify the torque from vessel motion; however, this is yet to produce a net power gain. Pendulums have been utilised extensively for harvesting this type of motion, converting ambient inertial vibration into rotation of a pendulum mass to drive a motor, usually relying on resonance. One such energy harvester specifically designed to power USVs has been demonstrated by Borowiec et al. [24], which uses a small pendulum coupled to DC motors through a rack and pinion. This device was previously tested by Mitcheson et al. [25], alongside a proposed system for altering the natural resonant frequency of the pendulum using power electronics, though this has had limited success with increasing power at any frequencies compared with the usual response. While compact, the rack and pinion used in this design limits the range of motion of the pendulum, and the use of two DC generators is inefficient and would increase the complexity of power management. On a larger scale, Marszal et al. [26] experimented with a parametrically excited pendulum-based energy harvester using a single one-way clutch and large flywheel. This study showed a low power to weight ratio with a mass of 5.07 kg and a maximum power of less than 0.5 W, perhaps due to the single clutch only harvesting half of the pendulum motion. More detailed analysis of parametric pendulum dynamics with respect to nonlinear behaviour has been given by Wiercigroch et al. [27]. Boren et al. [28] developed a pendulum in the form of a mass revolving around a vertical axis to convert wave motion to electricity. A further design was demonstrated by Liang et al. [29], with a bidirectional to unidirectional mechanical motion rectifier (MMR), using bevel gears and two one-way roller clutches, with the output gear driving a geared DC motor to generate power. This design appears to be the most promising of those reviewed, with a moderate power density, but bevel gears are not always efficient at handling large power, and are known to cause axial loads on one another which may affect the lifetime of the clutches used.

This work develops an alternative pendulum energy harvester with a completely novel mechanical rotation rectifier system, to harness the motion of USVs, which uses minimal spur gears through their offset layout for rectification of the input motion. Spur gears are the most reliable and often most efficient type of gear for this application, capable of transmitting large amounts of power with no axial thrust on their shafts. Two one-way sprag clutches are used to convert bidirectional input excitation into unidirectional rotation of a geared motor. These clutches are larger than the roller clutches often used in previous literature [29], and can transmit greater torque with extremely low backlash. These factors, along with a high torque, high gear ratio gearhead and efficient motor, are designed to allow this energy harvester to reliably transmit larger amounts of power than previous designs of this size. In addition, the simple design of the harvester enables changes to be made easily which allow it to be scaled to the required operating conditions. Scaling of the pendulum arm length, mass and flywheel inertia allow the resonant frequency, power level and amount of output rectification to be tuned with little or no alteration to the overall design. While the literature cited above demonstrates an array of significant research contributions which have helped to guide this research, it is difficult to compare the many harvesters as the physical properties of the devices and/or testing conditions and results are often incomplete in the writing. As such, a detailed quantitative comparison of device capabilities cannot be made, though the novelty and performance of the energy harvester proposed in this paper will be clear.

2. Description of energy harvester design

The overall design of the pendulum energy harvester is shown out of the vessel in Fig. 1(a), which consists of a pendulum frame, mass, mechanical rotation rectifier (MRR) and a geared motor with a flywheel, where the flywheel is present or not depending on the contribution to the output power, which will be discussed in Section 4.5. The longest shaft acts as a fixed centre of rotation across the width of the USV, secured at its ends into the hull, as shown in Fig. 1(b), such that the entire pendulum frame, when actuated by a pitching motion due to ocean waves, rotates about it. Having the entire assembly rotate allows the device to be easily mounted into the hull of a USV, while allowing the weight of the motor and gears to contribute to the mass of the pendulum. The bidirectional motion of the pendulum is transmitted to unidirectional rotation by the MRR specifically developed by the authors to increase the energy conversion efficiency of the DC motor generator. This unidirectional rotation drives the motor to produce electricity. The MRR is composed of two one-way-clutches and 4 offset spur gears.

The working mechanism of the MRR is shown in Fig. 2. On the long central shaft are two one-way clutches, mounted in opposing directions with gears fixed to the outer race of each, as shown in Fig. 2(a). The two smaller shafts each have a single gear fixed to them, meshing with each other, and arranged such that each is

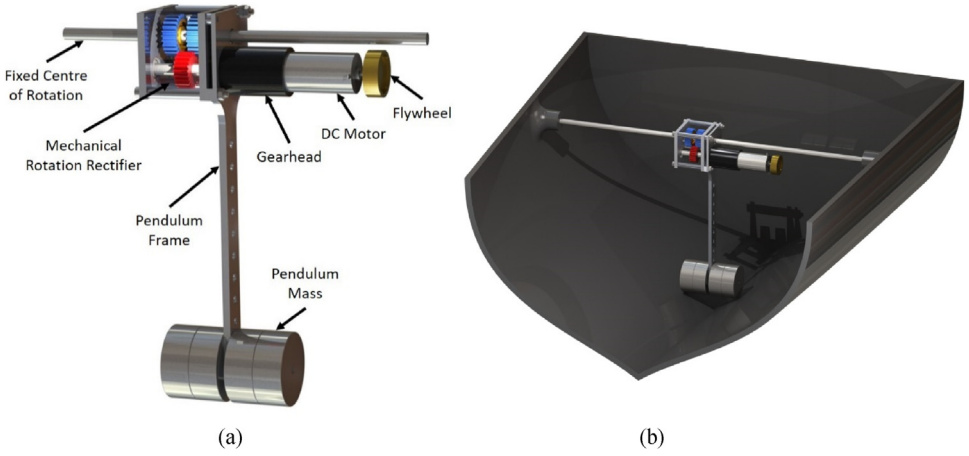

Fig. 1. Overall design of pendulum energy harvester: (a) out of vessel, and (b) on board, showing a section of a USV.

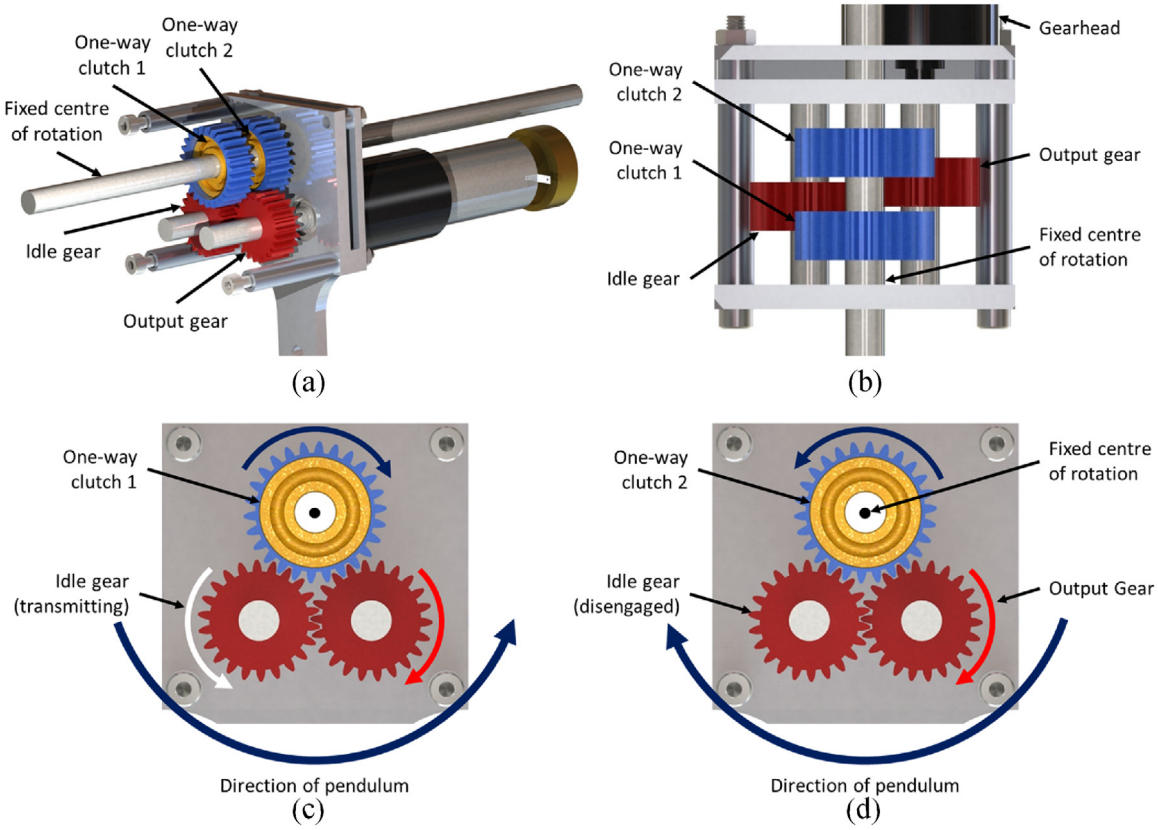

Fig. 2. CAD model demonstrating working mechanism of the pendulum energy harvester during operation: (a) 3D cut-away view of gearing assembly, (b) Top-down view of gearing, demonstrating spur gear offsets, (c) End view of gearing during anticlockwise direction of pendulum, and (d) End view of gearing during clockwise direction of pendulum.

in contact with one of the one-way clutches. The power transmission through these gears can be seen in Fig. 2(c & d), demonstrating the behaviour of the system during rotation of the pendulum arm in the anticlockwise and clockwise directions. It can be seen from this that in the anticlockwise direction (Fig. 2(c)), 'one-way clutch 1' engages, driving the 'idle gear' which in turn drives the 'output gear'. In the clockwise direction (Fig. 2(d)), 'one-way clutch 2' engages, driving the 'output gear' directly. This efficient use of minimal gears is made possible entirely by offsetting the gears from their usual planes, as is shown in Fig. 2(b). By keeping the number of gears to the least possible, the efficiency of the system is maximised and the backlash in the system minimised.

Due to the presence of clutches, when the input velocity of the pendulum is less than the output speed to the motor i.e. as the pendulum arm slows to a stop before changing direction, the clutches will freewheel and allow the motor to continue running without being slowed along with the input. This increases the power output of the system by (a) allowing the voltage output to remain greater than zero, hence continuing to produce power even when there is no input to the system due to the rotational momentum of the geared motor, and (b) ensuring that the motor is not forced to stall as the input velocity reaches zero, which would require significantly more torque to restart (and hence reduce power output) than to drive a motor which is already running in the same direction.

Scaling of the design is a simple process, involving a change of the pendulum mass and ensuring that the clutches and gearhead are capable of handling the torque provided by such a mass. Therefore, a higher power version would potentially require larger clutches and a higher torque gearhead, keeping the overall design intact. A lower power device could make use of smaller versions of all components and hence allow for a lighter and more compact harvester.

The DC motor used as the generator is a Maxon A-max 26, connected to a Maxon GP 32 A 103:1 planetary gearhead (Maxon Motor UK Ltd., Berkshire, UK). This motor was chosen for its low rotor inertia and stall torque, thus keeping the torque required to drive it to a minimum, and for its high efficiency and speed constant thus maximising the power produced by the motor at any given speed. The gearhead ratio was chosen to maintain the motor at a speed equal to or greater than its normal operating speed, with a planetary design used for its compact size and high torque capabilities. The gearhead is mounted to an end plate of the frame. The input to this gearhead is directly fixed into the output shaft, by means of turning a hole in the end of the output shaft and fixing the gearhead shaft inside using a grub screw. The pendulum arm is a long piece of aluminium plate with holes down its length, forming part of the frame, upon which the pendulum mass is fixed.

3. Mathematical modelling

A mathematical model of the pendulum energy harvester system has been developed to analyse the system. The purpose of this work is that, following the model verification with experimental results, it can be used to predict the performance of the device under various parameter changes and thus demonstrate its scalability and adaptability to different operating conditions.

A diagram of the pendulum system is shown in Fig. 3. The distance from the centre of the pendulum mass, m_M, to the pivot is l_M. The MRR, chassis, gear head and DC generator are represented together as a mass, m_P, with a distance of l_P from the pivot. A harmonic acceleration with an amplitude, A, and angular frequency,

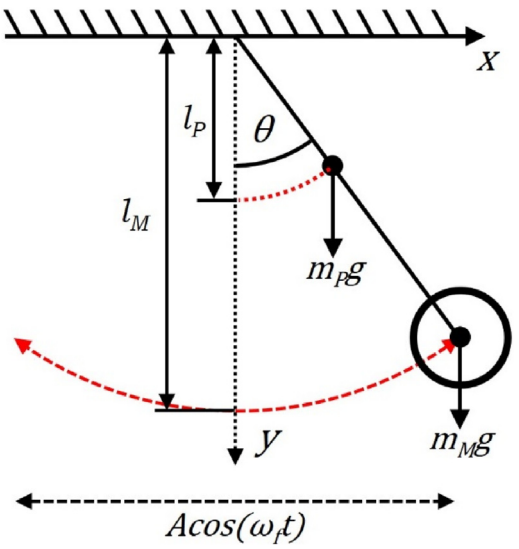

Fig. 3. 2D diagram of pendulum system.

ω_f, is applied along the *x*-axis. As a result, an angular displacement, θ, of the system is produced which drives the generator through the MRR and gearhead. As described in Section 2, the involvement of clutches in the system can lead to them freewheeling and hence the output disengages from the driving input. This means there are two states of the system:

1) Coupled: $\dot{\theta} n_S n_G \geq \dot{\theta}_{GB}$, while the generator is driven by the pendulum.
2) Uncoupled: $\dot{\theta} n_S n_G < \dot{\theta}_{GB}$,while the generator has no input applied to it.

where $\dot{\theta}$ is the angular velocity of the input pendulum arm, $\dot{\theta}_{GB}$ is the angular velocity of the motor output and gearhead, and n_S and n_G are the gear ratios of the spur gear MRR and gearhead, respectively.

a) Coupled System – Driven Output

When the pendulum system is coupled, the kinetic energy, *T*, of the system is:

$$T = \frac{1}{2}(J_P + J_M)\dot{\theta}^2 + \frac{1}{2}(J_F + J_G + J_{GB})\dot{\theta}_{GB}^2 \tag{1}$$

where J_P and J_M are the rotational inertia of the pendulum chassis and affixed mass with respect to pivot, and J_F, J_G, and J_{GB} are the rotational inertia of the flywheel, generator and gearbox with respect to their centre of rotation parallel to the z-axis, respectively. $\dot{\theta}_{GB}$ is the angular velocity of the generator and gearhead.

The potential energy, *V*, of the system is:

$$V = (m_P g l_P + m_M g l_M)\left(1 - cos\theta\right) \tag{2}$$

where m_P is the mass attached to the pendulum arm, at a distance l_P from the origin, and m_M is the mass of the pendulum chassis, with centre of mass l_M from the origin.

The non-conservative forces acting on the system are due to the input excitation from motion, and the back electromotive voltage of the generator. The back emf, V_G, from the generator is calculated as:

$$V_G = k_e \dot{\theta}_{GB} \tag{3}$$

where k_e is the known voltage constant of the motor used here as the electrical generator. The resistive torque produced by the generator with electrical current I_G is hence:

$$T_G = k_t I_G = \frac{k_t V_G}{R_i + R_L} = \frac{k_t k_e \dot{\theta}_{GB}}{R_i + R_L} = \frac{k_t k_e n_S n_G \dot{\theta}}{R_i + R_L} \tag{4}$$

where k_t is the known torque constant of the motor, and R_i and R_L are the internal resistance of the generator and attached external resistive load, respectively. n_S and n_G are the ratios of the spur gears and gearhead respectively. $\dot{\theta}_{GB}$ is the rotational speed of the generator, where $\dot{\theta}_{GB} = \dot{\theta} n_S n_G$.

The energy into the system is due to input excitation, which can be modelled as a sinusoidal input acting in the horizontal *x* plane. The generalised moment, *Q*, acting on the system, therefore, is:

$$Q = (m_M l_M + m_P l_P) A\, cos\theta \cos\left(\omega_f t\right) - \frac{k_t k_e {n_S}^2 {n_G}^2}{R_i + R_L}\dot{\theta} \tag{5}$$

Here, the electrical damping, c_E, can be defined as:

$$c_E = \frac{k_t k_e {n_S}^2 {n_G}^2}{R_i + R_L} \tag{6}$$

Calculating the Lagrange function, L = T – V, using Eqs. (1 and 2) and (5 and 6), and substituting into the following Lagrange equation:

$$\frac{d}{dt}\left(\frac{\partial L}{\partial \dot{\theta}}\right) - \frac{\partial L}{\partial \theta} = Q \tag{7}$$

The equation of motion of the system with added mechanical damping is:

$$(J_P + J_M + (J_F + J_G) n_s^2 n_G^2 + J_{GB} n_S^2)\ddot{\theta} + (c_E + c_{MP} + c_{MG})\dot{\theta} + (m_P l_P + m_M l_M) g\, sin\theta = (m_P l_P + m_M l_M)\, cos\theta\, A\cos\left(\omega_f t\right) \tag{8}$$

where c_{MP} and c_{MG} are the added mechanical damping of the pendulum side and gearbox/motor side of the system, respectively, separated by the clutches.

b) Decoupled System – Free Output

Consider now the time for which the pendulum arm is rotating at a slower rate than the driven spur gears. The clutches will freewheel and the input of the pendulum will be disconnected from the gearhead and generator. This leads to two decoupled systems: (a) the pendulum actuated by the input excitation, which can be described as in (9); (b) the free spinning of the spur gears, gearhead and generator, which is represented by (10). In this case, the condition for this decoupling is $\dot{\theta} n_S n_G < \dot{\theta}_{GB}$.

$$(J_P + J_M)\ddot{\theta} + c_{MP}\dot{\theta} + (m_P l_P + m_M l_M) g sin\theta = (m_P l_P + m_M l_M)\, cos\theta\, A\cos\left(\omega_f t\right) \tag{9}$$

$$\left((J_F + J_G) n_s^2 n_G^2 + J_{GB} n_S^2\right)\ddot{\theta} + (c_E + c_{MG})\dot{\theta} = 0 \tag{10}$$

c) Illustration of Combined System

The system was modelled from Eqs. (8)–(10), coded using MATLAB, which was then used to simulate and plot the response of the harvester. An illustration of Eqs. (8)–(10) can be seen in Fig. 4. Here, the pendulum input velocity, $\dot{\theta} n_S n_G$, is compared to the output velocity, $\dot{\theta}_{GB}$, clearly showing a decoupling of the two between the clutches disengaging and re-engaging. Table 1 gives a list of the physical parameters of the pendulum system, used as variables in the mathematical model to define the system for comparison to experimental results in Section 4.

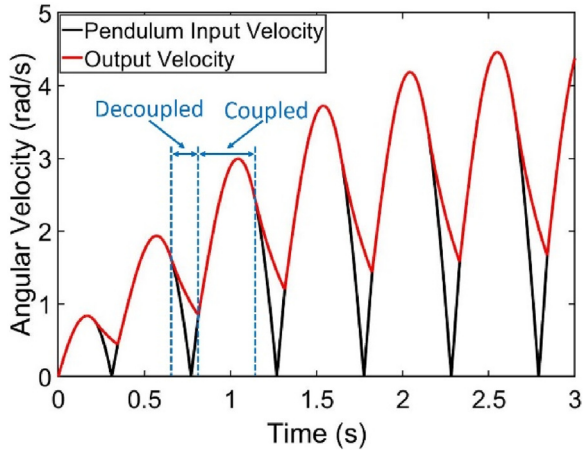

Fig. 4. Illustration of angular velocity of the system on either side of the clutches at start up, demonstrating decoupling of the system.

Table 1
Prototype energy harvester parameters.

Variable	Description	Value	Unit
J_P	Rotational inertia of chassis	3.5655×10^{-4}	kg·m^2
J_M	Rotational inertia of mass	0.0484	kg·m^2
J_F	Rotational inertia of flywheel	0 to 1.5×10^{-5}	kg·m^2
J_G	Rotational inertia of generator	1.25×10^{-6}	kg·m^2
J_{GB}	Rotational inertia of gearbox	9.1×10^{-7}	kg·m^2
m_P	Mass of chassis	0.674	kg
l_P	Distance from pivot to chassis centre of mass	0.023	m
m_M	Pendulum mass	1	kg
l_M	Length of pendulum arm	0.22	m
m_F	Mass of flywheel	0 to 0.075	kg
r_F	Radius of flywheel	0.02	m
k_e	Generator voltage constant	19.897	(Rad/s)/V
k_t	Generator torque constant	2.186×10^{-4}	Nm/V
R_i	Internal resistance of generator	30.1	Ω
R_L	Resistance of external electrical load	100 to 1500	Ω
n_S	Gear ratio of spur gears	26/22:1	–
n_G	Gear ratio of gearbox	103:1	–

4. Results and discussion

4.1. Experimental setup

The pendulum energy harvester was tested without a flywheel using the setup shown in Fig. 5. The central shaft of the harvester was fixed into a steel frame, which was secured to an APS 113 long stroke shaker via an auxiliary table kit (Techni Measure Ltd., Doncaster, UK). The shaker was excited via the combination of a signal function generator, set up to produce a sine wave of the desired frequency, and a power amplifier which used the generated signal as an input, with its output driving the shaker. The output terminals of the generator were connected to a load resistor. The acceleration produced by the shaker was measured via a Kistler 8762A5 accelerometer (Kistler Instruments Ltd., Hampshire, UK). The voltage outputs from the accelerometer and across the load resistor were measured using National Instruments Data Acquisition (DAQ) hardware, and recorded via LabVIEW software on a desktop computer. A LabVIEW program was used to calculate and record the cumulative energy produced by the system based on voltage and known resistive load, which was then used to calculate average power over a period by dividing the total energy by the time in seconds. Normalised voltage was then calculated by dividing the average voltage by the rms acceleration, and normalised power calculated by dividing the average power by the square of the rms acceleration.

4.2. Initial experimental results

Typical performance traces from experimental testing are shown in Fig. 6, with voltage, power and acceleration recorded simultaneously. The device has been tested at two different frequencies, 1 Hz and 2 Hz, and the results compared with those of the mathematical model to demonstrate its performance under different conditions. In the mathematical model, the mechanical damping coefficients c_{MP} and c_{MG} were varied until the sum of the absolute voltage errors between simulation and experiment across the frequency range of 0.5−2 Hz was minimised. The values of c_{MP} and c_{MG} minimising the voltage errors were found to be 0.041 and 0.022, respectively.

Something to note is that the major output voltage and power peaks every 0.5 s each have an extra smaller peak for 1 Hz. As seen from Fig. 6(a), the shaker is not able to produce an accurate sinusoidal acceleration at this low frequency, and it is this limitation which is causing the behaviour of the generator output. This is then overcome at 2 Hz, where the input acceleration resembles a near perfect sine wave. As can be expected, two alternating sets of major peaks in voltage and power are observed, where Set 1 peaks are higher than Set 2. The Set 1 peaks are produced when the pendulum rotates in the clockwise direction (Fig. 2(d)), where the driving gear meshes directly with the output gear. Set 2 peaks are produced when the pendulum rotates in the anticlockwise direction (Fig. 2(c)), which involves the additional meshing of the idle gear, introducing additional damping and backlash and hence leading to a slight reduction in output voltage and power. Although the input excitation takes a sinusoidal form, i.e. the speed of the pendulum arm crosses zero, the output voltage is always larger than zero. This is due to the freewheel of the clutches when the pendulum arm speed is less than the output speed to the motor, allowing the motor to continue running without being slowed with the pendulum arm. It can also be seen that the simulation results are very accurate at 1 Hz, but underestimate the voltage and hence power at 2 Hz. This is because the damping coefficients in simulation were selected to minimise the sum of the errors between simulation and experiment across the frequency range from 0.5 to 2 Hz. As a result, the errors between simulation and experiment can vary at different frequencies.

4.3. Determining optimal load

To determine the optimal load resistor for the pendulum energy harvester, the voltage was measured across a range of external loads at 1 Hz. The average power was then calculated by recording the total energy produced over a 10 s period and dividing by 10. The input excitation was maintained at 0.18 g and the average power at each load resistor was normalised over input acceleration, as shown in Fig. 7. The pendulum energy harvester produces the maximum power of 20.62 W/g^2 when a 900 Ω load resistor is connected. In the frequency range of interest in this study, the optimal load of 900 Ω is expected to remain unchanged and therefore was used for all further testing.

4.4. Final system experimental results

Repeating the same experiment as in Fig. 6, now with the optimal load of 900 Ω, the response of the energy harvester at resonance can be obtained, as shown in Fig. 8.

Using the optimal load resistor, the average voltage and power of the energy harvester was measured between 0.5 Hz and 2 Hz. The input displacement was maintained at the maximum displacement

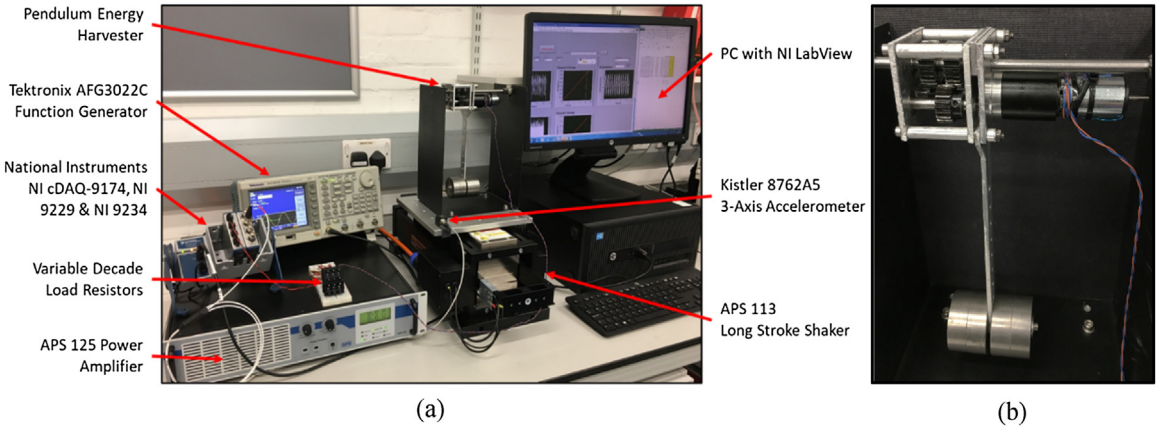

Fig. 5. (a) Experimental setup for testing energy harvester prototype and (b) prototype pendulum energy harvester without a flywheel.

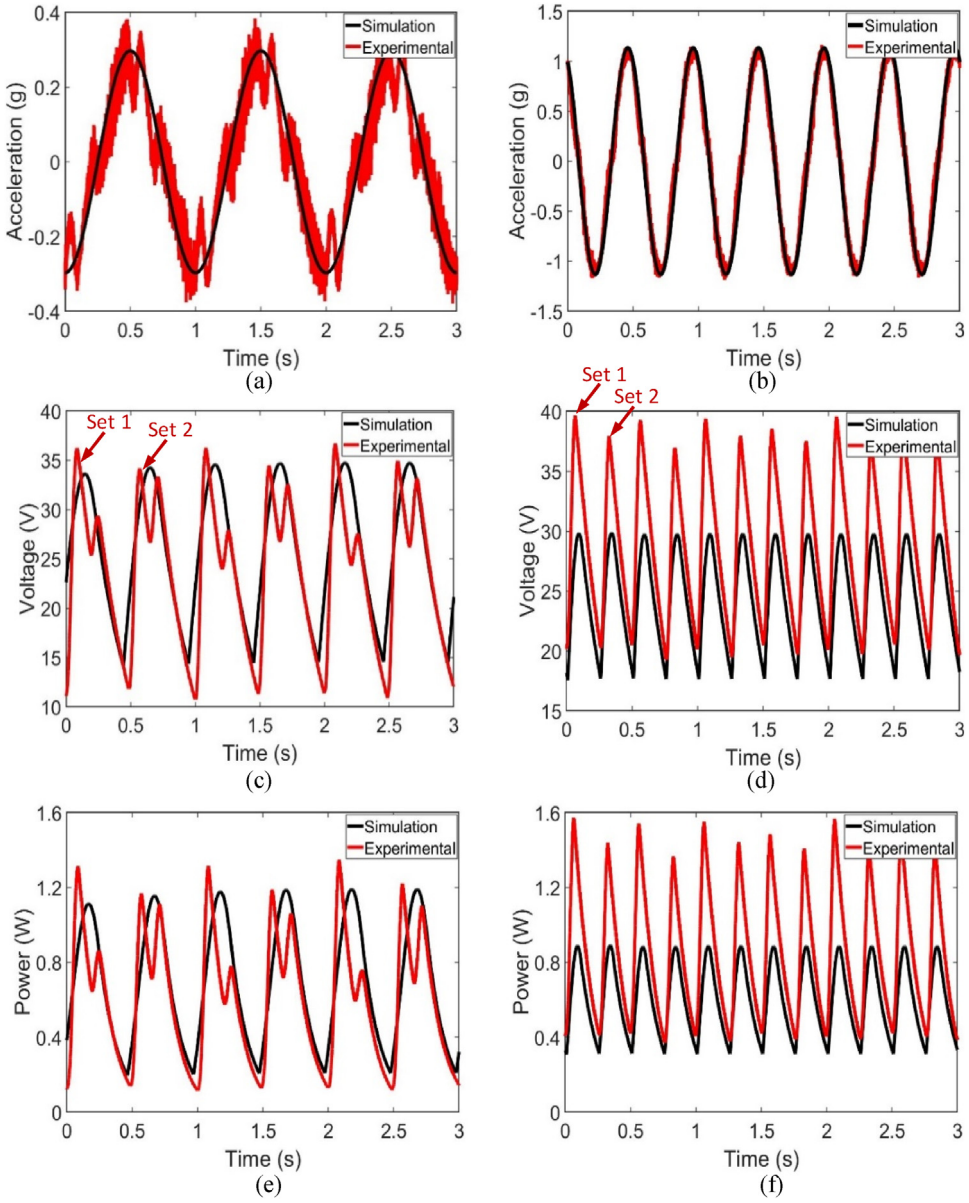

Fig. 6. Comparison of measured experimental and simulation results of pendulum energy harvester with 1000 Ω load and with $m_F = 0$, where (a) & (b) input acceleration, (c) & (d) corresponding instantaneous voltage output of harvester, and (e) & (f) corresponding instantaneous power output of harvester, when actuated at 1 Hz and 2 Hz respectively.

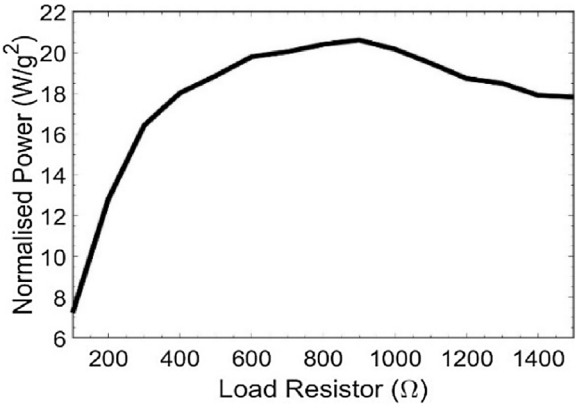

Fig. 7. Normalised average power output of the energy harvester connected to different load resistances, when actuated at 1 Hz and $m_F = 0$.

of the shaker, at 150 mm peak to peak. The acceleration at different frequencies was therefore not constant, as the displacement was fixed across all frequencies. To compare the output at different frequencies, the voltage and power are normalised over acceleration and the square of acceleration, respectively, in accordance with known proportional relationships between these readings and acceleration [30]. The normalised average voltage and power responses of the energy harvester are shown in Fig. 9(a & b). The corresponding simulation results are also provided for comparison.

The simulation results show an accurate resemblance to the experimental results, with some minor discrepancies in performance at frequencies higher than resonance. The pendulum energy harvester clearly has a resonant frequency at 1 Hz, at which it produces the normalised maximum voltage of 136.2 V/g and normalised average power of 20.62 W/g^2. When actuated at an acceleration of 0.186 g rms, the pendulum energy harvester produced peak voltage of 37 V and peak power of 1.4 W. The average voltage and power are 25.44 V and 0.72 W, respectively. Considering the overall mass of the system of 1.674 kg, this gives a power density of 0.43 W/kg, or a normalised power density of 12.32 W/g^2/kg. Table 2 compares the performance of low-frequency vibration energy harvesters. The pendulum energy harvester developed in this study has a higher normalised power density.

Considering now the efficiency of the system, the energy into the harvester can be compared with the measured electrical energy out. In this case, the input energy into the system is due to the motion of the shaker, and the energy out can be determined from the measured output power of the system during testing. The input energy provided by the shaker can be estimated by using the known input torque due to the moving pendulum mass:

$$T = (m_P l_P + m_M l_M)\cos\theta A\cos\left(\omega_f t\right) \tag{11}$$

Integrating the product of this torque with angular displacement of the pendulum arm, the input energy to the system can be calculated for a particular frequency. At 1 Hz, this produces an input energy of 1.66 J per second. The output energy from the harvester in one second is known to be 0.72 J, giving a system efficiency of 43.5 % from input vibration to output power, at resonance.

4.5. Effects of key harvester parameters

This section investigates the variation of key energy harvester parameters in order to determine their effect on performance and to illustrate the potential to optimise the device for different applications. The key parameters are the pendulum arm length, pendulum mass, and flywheel inertia, and these are all varied

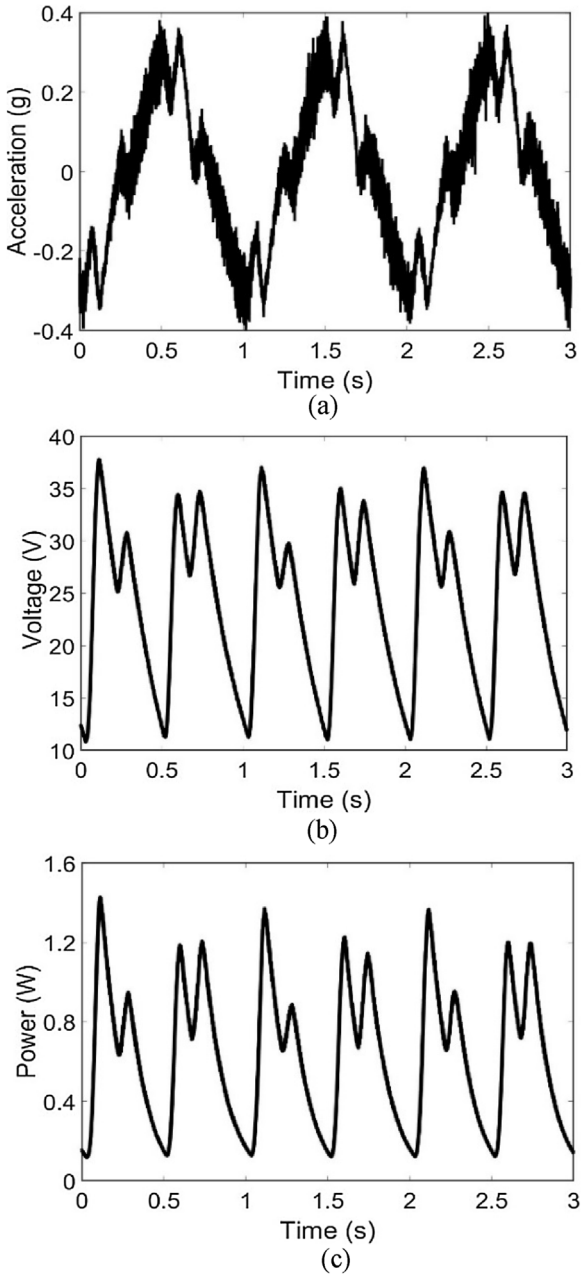

Fig. 8. Measured instantaneous voltage and power output from generator when connected to a 900 Ω load at 1 Hz excitation with 0.18 g rms acceleration and $m_F = 0$ kg.

within the mathematical model and the corresponding performance of the harvester is simulated in each case. They were chosen to be varied because they were expected to have the most significant effects on the device performance, and to be practical to change without making major alterations to the energy harvester.

a) Effect of Pendulum Arm Length

First, the energy harvester was tested experimentally using a different pendulum arm length from the initial test of 0.145 m, with the results compared to the simulation in order to verify that the mathematical model is accurate at different arm lengths, as shown in Fig. 10. The normalised power output of the harvester was then simulated in the frequency domain across a range of pendulum arm lengths, from 0.1 m to 0.3 m, shown in Fig. 11. As expected,

Table 2
Performance comparison of low-frequency vibration energy harvesters.

Energy Harvester	Type	Frequency (Hz)	Acceleration (g)	Inertial Mass (kg)	Power (mW)	NPD (W/g^2/kg)
Graves et al.	EM	1	0.186	1.6	720	12.32
Liang et al. [29]	EM	1	–	0.36	–	1.6
Saha et al. [31]	EM	2.5	1	0.027	1.86	0.069
Kuang et al. [10]	EM	5.8	0.2	0.014	1.31	2.37
Arakawa et al. [32]	ES	10	0.40	0.7×10^{-3}	6×10^{-3}	0.054

Types: EM - electromagnetic; ES - electrostatic.

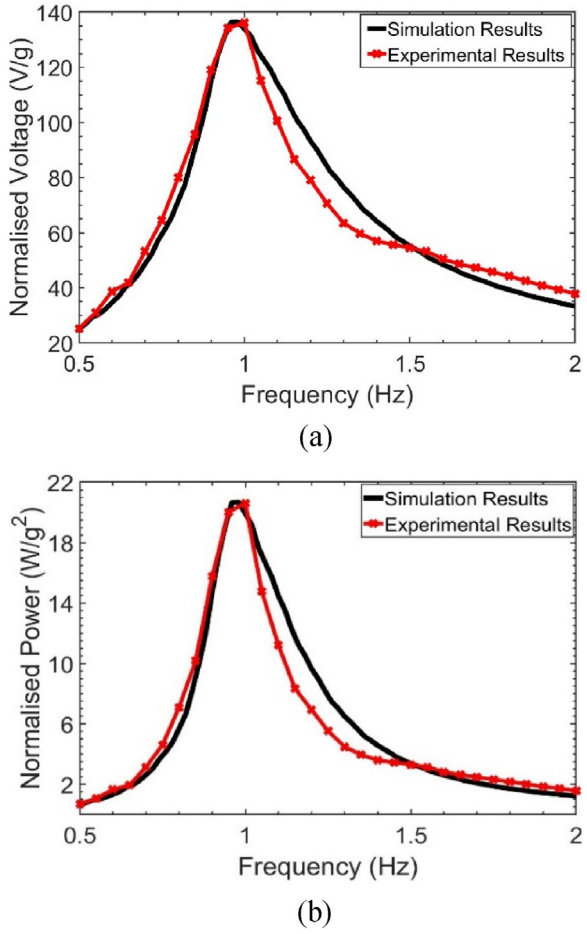

Fig. 9. (a) Normalised average voltage and (b) normalised average power output of pendulum energy harvester when connected to a 900 Ω external load and m_F = 0 kg.

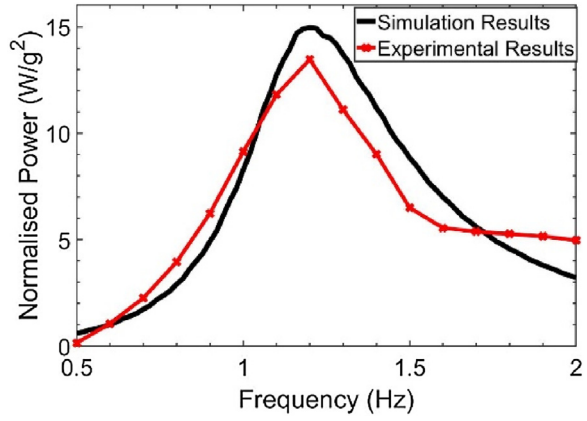

Fig. 10. Normalised average power output of pendulum energy harvester when connected to a 900 Ω external load, l_M = 0.145 m, m_M =1.0 kg and m_F = 0 kg.

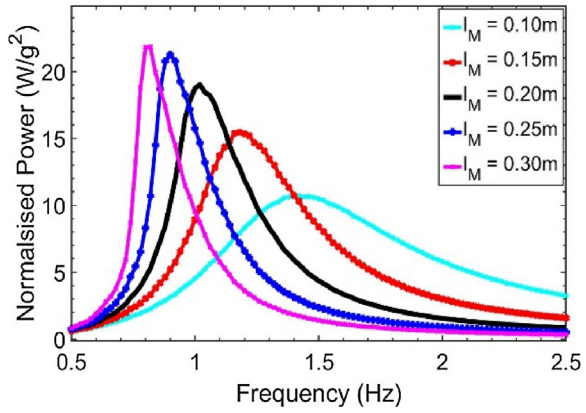

Fig. 11. Simulated resonant frequency of pendulum energy harvester compared with pendulum arm length, when connected to a 900 Ω external load, m_M =1 kg and m_F = 0 kg.

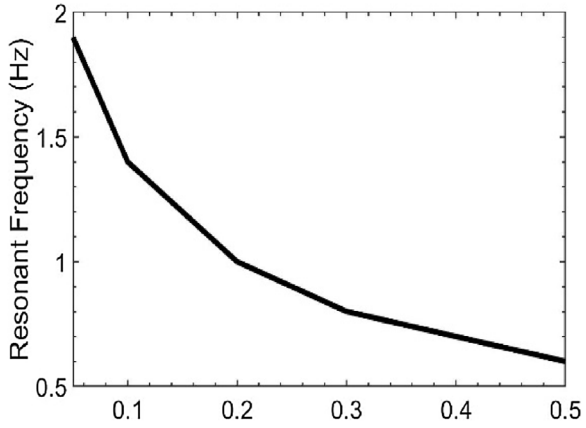

Fig. 12. Simulated normalised average power output of pendulum energy harvester with varying pendulum arm length, when connected to a 900 Ω external load, m_M =1.0 kg and m_F = 0 kg.

this clearly shows the resonant frequency of the device decreasing with increasing arm length, which is a commonly known trait of pendulums. In addition, the bandwidth was also reduced as the arm length is increased. The relationship between resonant frequency and pendulum arm length can be drawn from this, and is shown in Fig. 12, thus allowing the natural frequency of the device to be easily tuned to a range of frequencies dependant on the operating conditions, by scaling the arm length.

b) Effect of Pendulum Mass

The effects of the pendulum mass were investigated using the same method, again starting with experimentally validating the model using a different pendulum mass from the initial test of 0.75 kg, as shown in Fig. 13. The output power from the device was then simulated across different masses, from 0.5 kg to 1.5 kg, as in Fig. 14. This shows the increase in power as the pendulum

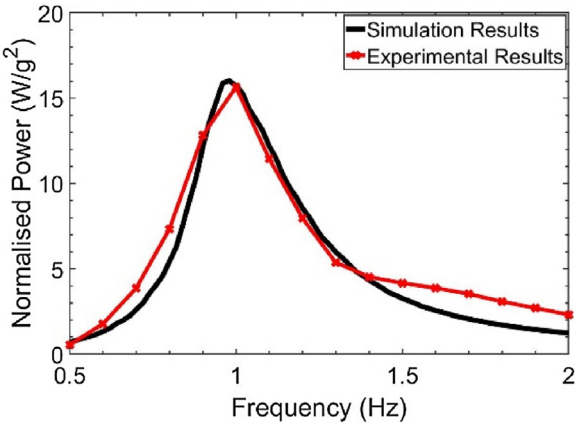

Fig. 13. Simulated average power output of pendulum energy harvester with varying pendulum mass, when connected to a 900 Ω external load, l_M = 0.22 m and m_F = 0 kg.

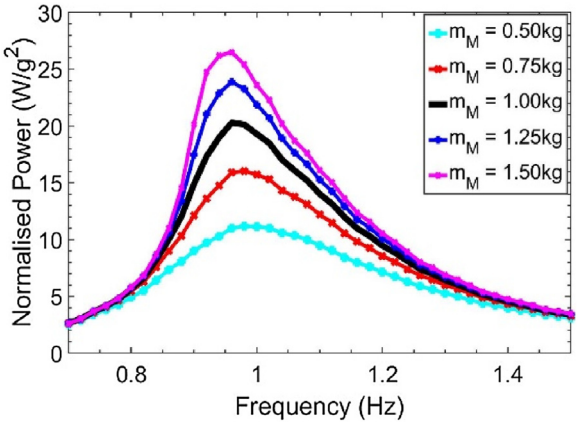

Fig. 14. Average power output of pendulum energy harvester when connected to a 900 Ω external load, l_M = 0.22, m_M = 0.75 kg and m_F = 0.

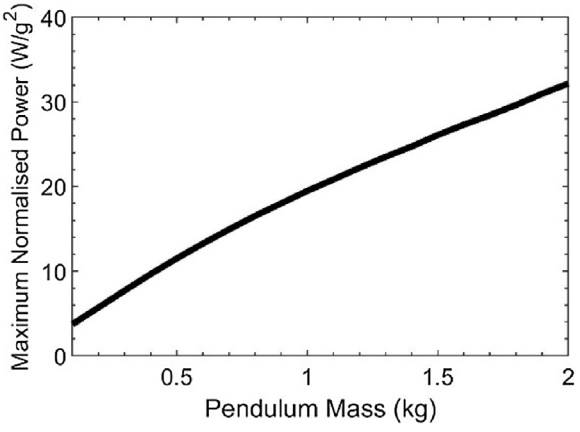

Fig. 15. Simulated maximum average power output of pendulum energy harvester with different pendulum masses, when connected to a 900 Ω external load, l_M = 0.22 m and m_F = 0 kg.

mass is increased, with little to no effect on the resonant frequency. Fig. 15 illustrates the relationship between the peak maximum normalised power and the pendulum mass, with each data point simulated with corresponding optimal external load. This demonstrates another part of the design which is clearly scalable, enabling the device to match various power demands. It is also important to note that scaling up to a larger pendulum mass would lead to little or no increase in the mass of the chassis. Since the power of the system is almost entirely dependent on the affixed weights, increasing m_M would lead to higher power gains compared to the proportionate increase in mass. Therefore, larger versions of this device would have greater power density, and it can be scaled up to produce power in the range of multiple watts thus making it a viable energy source for USVs.

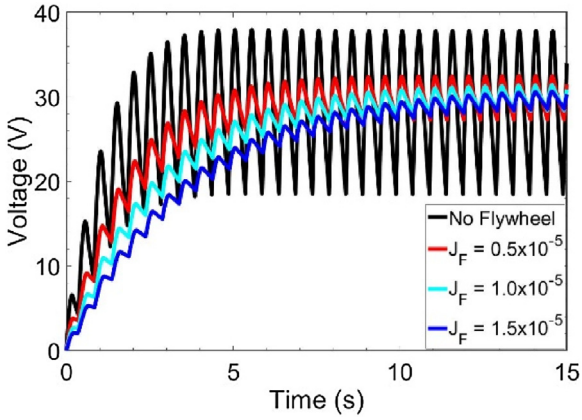

Fig. 16. Simulated voltage output of pendulum energy harvester at start up when connected to a 900Ω external load and excited at 1 Hz, with various flywheels.

c) Effect of Flywheel Inertia

With a large proportion of existing studies of pendulum energy harvesters including a fixed flywheel [26,29], the system in this work was tested without to accurately determine a baseline performance for the device. The performance of the harvester with flywheels of different inertia was explored using simulation. The simulated transient responses of the energy harvester are shown in Fig. 16. As the inertia of the flywheel increases, the time to reach a steady state is also increased. With no flywheel, the time to reach a steady state is around 3 s, rising up to approximately 14 s for $J_F = 1.5 \times 10^{-5}$ kg·m^2. Although a higher inertia of the flywheel leads to a longer transient time, it produces a smoother output not just in the transient process, but also at steady state, as shown in Fig. 17. Without a flywheel, the voltage output varies between 17 and 37 V; with $J_F = 1.5 \times 10^{-5}$ kg·m^2, the variation is reduced to between 27 and 30 V. The effects of the flywheel on the power output of the pendulum energy harvester at different excitation frequency is presented in Fig. 18. The flywheel slightly increases both the resonant frequency and power output. This is likely due to the reduced damping ratio resulting from the increased inertia and unchanged damping coefficients.

5. Conclusion

In this study, a pendulum energy harvester with a mechanical rotation rectifier (MRR) has been designed, modelled, prototyped and characterised to harvest low frequency ambient vibration, generated by ocean waves to supply power for unmanned surface vehicles. The energy harvester employs a novel MRR design involving offset gears and clutches, allowing the use of a minimal number of spur gears to maximise efficiency and reduce the backlash of the transmission line while maintaining high torque capabilities. This design has been accurately 3D modelled in detail and fabricated in an all-metal construction. Testing the device with varying externally connected electrical loads concluded that 900 Ω was the optimal resistor for maximum power out of the system at the resonant frequency of 1 Hz. Carrying out frequency sweeps on the device under this connected load demonstrated a maximum

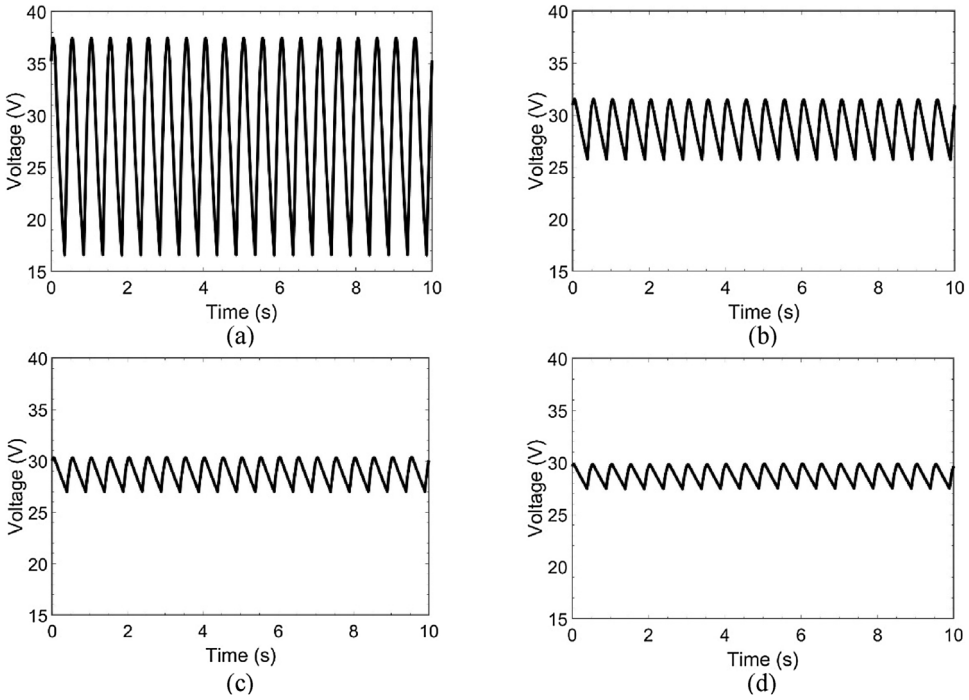

Fig. 17. Simulated voltage output of energy harvester during steady state when connected with a 900 Ω external load and excited at 1 Hz, with different flywheel inertias: (a) $J_F = 0$, (b) $J_F = 0.5 \times 10^{-5}$ kg·m^2 (c) $J_F = 1.0 \times 10^{-5}$ kg·m^2, and (d) $J_F = 1.5 \times 10^{-5}$ kg·m^2.

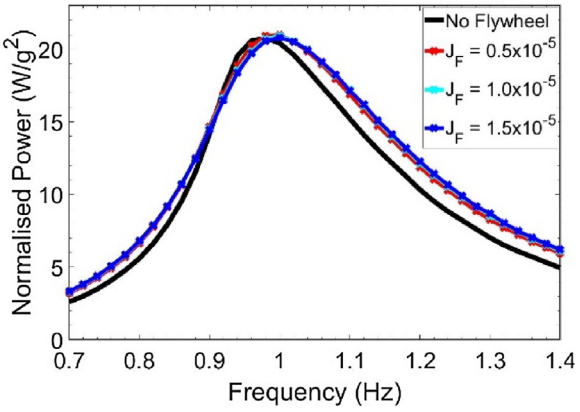

Fig. 18. Simulated average power output of pendulum energy harvester connected to a 900 Ω external load with various flywheels.

normalised power output of 20.62 W/g^2, corresponding to 0.72 W at 0.186 g rms acceleration, giving an overall power density of 0.43 W/kg, or 12.32 W/g^2/kg, and a maximum efficiency from input excitation to electrical power output of 43.5 %. The 1 Hz resonant frequency of the device lies within the expected natural frequency range of marine vessels, and could be further tuned to match the specific needs of a particular vessel. A mathematical model has been derived with consideration of the coupled and decoupled states of the system to simulate and predict the response and performance of the device to a given sinusoidal input vibration. The mathematical model correlated well with the experimental results. This paper went a step further and carried out simulation analysis of the effects of varying three key device parameters of the pendulum, showing the specific relationships between pendulum arm length and natural frequency, and pendulum mass and maximum power. In addition, the effects of different flywheels were investigated, demonstrating a clear smoothing of the voltage at higher flywheel inertias, as well as an overall increase in power during steady state at the expense of extended start up time. This device has the potential to assist in powering USV communications at its current size, but can be easily scaled up to produce power in the range of multiple watts and thus providing an effective source of energy for extending the duration of exploration for USVs.

CRediT authorship contribution statement

James Graves: Conceptualization, Methodology, Software, Validation, Formal analysis, Investigation, Writing - original draft, Writing - review & editing, Visualization. **Yang Kuang:** Methodology, Formal analysis, Resources, Writing - review & editing, Supervision. **Meiling Zhu:** Resources, Writing - review & editing, Supervision, Project administration, Funding acquisition.

Declaration of Competing Interest

The authors declare that they have no known competing financial interests or personal relationships that could have appeared to influence the work reported in this paper.

Acknowledgement

This research is funded by the EPSRC Standard Research Studentship (DTP), Grant No. EP/R512254/1.

References

[1] N.C. Townsend, Self-powered autonomous underwater vehicles: results from a gyroscopic energy scavenging prototype, IET Renew. Power Gener. 10 (8) (2016) 1078–1086.
[2] Y. Yin, D. Zhao, H. Cui, M. Hong, Predicting method of natural frequency for ship's vertical vibration, Brodogradnja 65 (3) (2014) 49–58.
[3] N. Wu, Q. Wang, X. Xie, Ocean wave energy harvesting with a piezoelectric coupled buoy structure, Appl. Ocean. Res. 50 (2015) 110–118.
[4] A. Jbaily, R.W. Yeung, Piezoelectric devices for ocean energy: a brief survey, J. Ocean. Eng. Mar. Energy 1 (1) (2015) 101–118.
[5] Y. Kuang, et al., Energy harvesting during human walking to power a wireless sensor node, Sens. Actuators A Phys. 254 (2016).

[6] W.S. Hwang, et al., Design of piezoelectric ocean-wave energy harvester using sway movement, Sens. Actuators A Phys. 260 (2017) 191–197.
[7] J. Chen, et al., Networks of triboelectric nanogenerators for harvesting water wave energy: a potential approach toward blue energy, ACS Nano 9 (3) (2015) 3324–3331.
[8] Z.L. Wang, Triboelectric nanogenerators as new energy technology and self-powered sensors - Principles, problems and perspectives, Faraday Discuss. 176 (0) (2014) 447–458.
[9] Y. Jia, et al., Real world assessment of an auto-parametric electromagnetic vibration energy harvester, J. Intell. Mater. Syst. Struct. 29 (7) (2017) 1481–1499.
[10] Y. Kuang, R. Hide, M. Zhu, Broadband energy harvesting by nonlinear magnetic rolling pendulum with subharmonic resonance, Appl. Energy 255 (2019) 113822.
[11] K. Fan, et al., A string-suspended and driven rotor for efficient ultra-low frequency mechanical energy harvesting, Energy Convers. Manage. 198 (2019) 111820.
[12] P. Li, et al., A magnetoelectric energy harvester and management circuit for wireless sensor network, Sens. Actuators A Phys. 157 (1) (2010) 100–106.
[13] X. Dai, An vibration energy harvester with broadband and frequency-doubling characteristics based on rotary pendulums, Sens. Actuators A Phys. 241 (2016) 161–168.
[14] N.G. Stephen, On energy harvesting from ambient vibration, J. Sound Vib. 293 (1) (2006) 409–425.
[15] F. Cottone, H. Vocca, L. Gammaitoni, Nonlinear energy harvesting, Phys. Rev. Lett. 102 (8) (2009) 080601.
[16] Z. Lei, T. Xiudong, Large-scale vibration energy harvesting, J. Intell. Mater. Syst. Struct. 24 (11) (2013) 1405–1430.
[17] E. Al Shami, R. Zhang, X. Wang, Point absorber wave energy harvesters: a review of recent developments, Energies 12 (1) (2018) 47.
[18] B. Drew, A. Plummer, M. Sahinkaya, A review of wave energy converter technology, Arch. Proc. Inst. Mech. Eng. Part A J. Power Energy 223 (2009) 887–902.
[19] T. Lin, et al., Modeling and field testing of an electromagnetic energy harvester for rail tracks with anchorless mounting, Appl. Energy 213 (2018) 219–226.
[20] Y. Yuan, et al., Design and treadmill test of a broadband energy harvesting backpack with a mechanical motion rectifier, J. Mech. Des. 140 (8) (2018), p. 085001-085001-085008.
[21] Q. Xie, et al., A novel oscillating buoy wave energy harvester based on a spatial double X-shaped mechanism for self-powered sensors in sea-crossing bridges, Energy Convers. Manage. (2019) 112286.
[22] X. Tang, L. Zuo, Vibration energy harvesting from random force and motion excitations, Smart Mater. Struct. 21 (7) (2012) 075025.
[23] L.C. Rome, et al., Generating electricity while walking with loads, Science 309 (5741) (2005) 1725.
[24] M. Borowiec, et al., Dynamic response of a pendulum-driven energy harvester in the presence of noise, J. Phys. Conf. Ser. 476 (2013) 012038.
[25] P.D. Mitcheson, et al., Tuning the resonant frequency and damping of an electromagnetic energy harvester using power electronics, IEEE Trans. Circuits Syst. II Express Briefs 58 (12) (2011) 792–796.
[26] M. Marszal, et al., Energy harvesting from pendulum oscillations, Int. J. Non. Mech. 94 (2017) 251–256.
[27] M. Wiercigroch, A. Najdecka, V. Vaziri, Nonlinear Dynamics of Pendulums System for Energy Harvesting, Dordrecht: Springer, Netherlands, 2011.
[28] B.C. Boren, B.A. Batten, R.K. Paasch, Active control of a vertical axis pendulum wave energy converter, 2014 American Control Conference (2014).
[29] L. Changwei, W. You, Z. Lei, Broadband pendulum energy harvester, Smart Mater. Struct. 25 (9) (2016) 095042.
[30] S. Roundy, P.K. Wright, J. Rabaey, A study of low level vibrations as a power source for wireless sensor nodes, Comput. Commun. 26 (11) (2003) 1131–1144.
[31] C.R. Saha, et al., Electromagnetic generator for harvesting energy from human motion, Sens. Actuators A Phys. 147 (1) (2008) 248–253.
[32] Y. Arakawa, Y. Suzuki, N. Kasagi, The Proceedings of the National Symposium on Power and Energy Systems, 2004, Micro seismic power generator using electret polymer film, 9, 2004.

Biographies

James Graves received his M.Eng in Electronic Engineering with Industrial Experience from University of Exeter in 2017. He is currently working towards his PhD in Energy Harvesting, with a focus on extending the operational time of unmanned surface vehicles through the implementation of low frequency vibration energy harvesting transducers.

Yang Kuang received his B.Eng and M.Eng in Mechanical Engineering from Central South University, China, in 2007 and 2010, respectively, and his PhD in high power piezoelectric transducers from University of Dundee in 2014. He is currently working as a research fellow in the energy harvesting research group in University of Exeter. His main research interests are focused on self-power wireless sensing systems enabled by energy harvesting.

Meiling Zhu received the B.Eng., M.Eng., and Ph.D. degrees from Southeast University, Nanjing, China, in 1989, 1992, and 1995, respectively. She is currently a Professor and the Chair of Mechanical Engineering and the Head of the Energy Harvesting Research Group with the University of Exeter, U.K. Her current research is concentrated on piezoelectric energy harvesting powered wireless communication and sensor nodes.